

Sunburst quantum Ising model under interaction quench: entanglement and role of initial state coherence

Akash Mitra^{1,2} and Shashi C. L. Srivastava^{1,2}

¹Variable Energy Cyclotron Centre, 1/AF Bidhannagar, Kolkata 700064, India

²Homi Bhabha National Institute, Training School Complex, Anushaktinagar, Mumbai - 400094, India

We study the non-equilibrium dynamics of an isolated bipartite quantum system, the sunburst quantum Ising model, under interaction quench. The pre-quench limit of this model is two non-interacting integrable systems, namely a transverse Ising chain and finite number of isolated qubits. As a function of interaction strength, the spectral fluctuation property goes from Poisson to Wigner-Dyson statistics. We chose entanglement entropy as a probe to study the approach to thermalization or lack of it in post-quench dynamics. In the near-integrable limit, as expected, the linear entropy displays oscillatory behavior while in the chaotic limit, it saturates. Along with the chaotic nature of the time evolution generator, we show the importance of the role played by the coherence of the initial state in deciding the nature of thermalization. We further show that these findings are general by replacing the Ising ring with a disordered XXZ model with disorder strength putting it in the many-body localized phase.

I. INTRODUCTION

There has been an upsurge of studies in the last decade, both theoretically and experimentally, to understand fundamental questions like relaxation dynamics and thermalization in out-of-equilibrium isolated quantum systems. Traditional quantifiers like two-point or higher order correlations of local operators and quantum information theoretic measures like entanglement entropy and out-of-time ordered correlators, among others, have been used as probes to understand whether the system attains the steady state, what is the nature of equilibrium or what is the path to achieve the same. The equilibrium state is described by Generalized Gibbs ensemble (GGE) or eigenstate thermalization hypothesis (ETH) depending on the system being integrable or quantum chaotic[1–12]. ETH essentially asserts that each energy eigenstate behaves like a micro-canonical ensemble [13–15]. Several analytical and numerical studies have shown that generic isolated quantum chaotic many-body systems relax to a state in which local observables achieve a time-independent value predicted by thermal distribution and are independent of the initial state as long as they are chosen from a small band of considered energy[16–20]. A generic approach for creating a system that does not thermalize is provided by many-body localization (for further information, see the reviews [21–23] and references therein). Another notable exception occurs when a many-body interacting system exhibits persistent revivals for specific initial states from the middle of the spectrum while exhibiting ergodicity for others. These specific initial states are called many-body scarred states [24, 25].

The dynamics of bipartite subsystem entanglement entropy following a quantum quench that drives the system away from its initial equilibrium state provides an equivalent method for studying thermalization in many-body systems. The Von Neumann entropy is one of the most commonly used entanglement measures in quantum in-

formation theory; however, we choose linear entropy for the ease of the calculation as well as being accessible to experimental measurements [11]. A many-body system can be imagined as a bipartite system with interaction strength between the two parts as a natural candidate for the quench parameter. The quench protocol for Hamiltonian is written as,

$$H = \begin{cases} H_A \otimes \mathbb{1}_B + \mathbb{1}_A \otimes H_B & t < 0 \\ H_A \otimes \mathbb{1}_B + \mathbb{1}_A \otimes H_B + V_{AB} & t \geq 0 \end{cases} \quad (1)$$

where $H_{A(B)}$ is Hamiltonian of subsystem $A(B)$ and V_{AB} is the interaction between the two. Time is denoted by t .

When H_A, H_B , as well as post-quench Hamiltonian H , is integrable, the analytical understanding of entanglement evolution comes from quasiparticle picture [26]. A phenomenological model which rather successfully predicts the entanglement between two subsystems at time t in terms of the number of intersecting trajectories of quasiparticles produced at time $t = 0$ in two subsystems. The entanglement entropy grows linearly in time before saturating to volume law entanglement [27–38]. In the other scenario, when H_A, H_B , as well as post-quench Hamiltonian H , are quantum chaotic, a random matrix theory-based approach explains the entanglement dynamics [39]. The quantum chaotic nature of subsystems is crucial in this approach as all the fluctuation and entanglement properties have been calculated by modeling subsystem Hamiltonian with suitable random matrix ensemble [39–45]. It motivates us to study the third scenario where pre-quench subsystems are integrable and interaction quench breaks the integrability of the post-quench system. The present study departs from the two previously studied scenarios as the integrability of subsystems forbids a random matrix theory-based approach. However, we can also not use a quasiparticle picture due to the quantum chaotic nature of the post-quench Hamiltonian. For this class of systems in which the total system is quantum chaotic due to coupling between the two in-

tegrable systems, it is a valid question to ask whether the equilibrium state of any of the two subsystems behaves like a thermal state or it can be characterized by GGE as is expected for integrable systems.

For the second scenario discussed above, where subsystems are modeled by corresponding random matrix ensemble, the initial coherence of the quantum state, defined as the sum of the square of off-diagonal elements of the density matrix written in energy basis, under interaction quench is shown to act as a resource for equilibration or thermalization even when the ETH is not satisfied [46]. The equilibration is called strong or weak depending on whether the initial state averaged temporal fluctuation of linear entropy is small or not. The equilibration will be referred to as thermalization whenever the equilibrium value of linear entropy reaches the corresponding random vector value, henceforth called Lubkin value[47]. For a random vector chosen uniformly from Hilbert space $\mathcal{H}_A \otimes \mathcal{H}_B$ of dimension 2^{L+n} with dimension of $\mathcal{H}_{A(B)}$, $2^L(2^n)$ such that $L \gg n$, the linear entropy of the either subsystem is $\approx 1 - \frac{1}{2^n}$.

In this paper, we study the spectral fluctuation of the static sunburst quantum Ising model [48] and show a transition from Poisson to Wigner-Dyson statistics as a function of interaction strength. Then, using linear entropy as a probe, we study the entanglement dynamics of qubits under interaction quench. We also show how initial state coherence plays a role in achieving strong thermalization under interaction quench. The key differences from the existing literature are as follows:

- In the bipartite setting shown in Eq. 1, the pre-quench limit of the *quantum chaotic* system is two non-interacting integrable subsystems in contrast to the non-integrable limit studied in the literature [39–42, 46].
- The coherence of the initial state is shown to control the mean and variance of the post-quench equilibrium value of the linear entropy.

The paper is organized as follows: We recollect the details of the sunburst quantum Ising model and results relevant to the present work in Section II, then study the transition from integrability to chaos with varying interaction strength between the Ising ring and qubits in Section III. We discuss the post-quench entanglement dynamics following the interaction quench in Section IV, while Section V focuses on the role of the initial state coherence in controlling the nature of thermalization. We present the summary and outlook in Section VI.

II. MODEL

We study a recently proposed sunburst quantum Ising model that is composed of a transverse field Ising ring, symmetrically coupled to a few isolated external qubits [48]. The subsystems *A* and *B* in Eq.1 correspond to the

transverse field Ising model and isolated qubits, respectively. The total Hamiltonian of this model is

$$H = H_I \otimes \mathbb{1}_q + \mathbb{1}_I \otimes H_q + V_{Iq}, \quad (2)$$

where H_I, H_q are Hamiltonian of transverse field Ising ring, isolated qubits respectively and V_{Iq} is the interaction term. $\mathbb{1}_{q(I)}$ is the identity operator in the space of qubits (Ising ring). The individual terms are defined as,

$$\begin{aligned} H_I &= - \sum_{i=1}^L (J\sigma_i^x \sigma_{i+1}^x + h\sigma_i^z) \\ H_q &= -\frac{\delta}{2} \sum_{i=1}^n \Sigma_i^z; \quad V_{Iq} = -\kappa \sum_{i=1}^n \sigma_{1+(i-1)b}^x \Sigma_i^x \end{aligned} \quad (3)$$

where L is the number of lattice points in the Ising ring and $\sigma_i^{x(z)}$ denotes Pauli matrices on the i th site. Note that both subsystems are integrable. Due to the ring topology of Ising, $\sigma_{L+1}^x = \sigma_1^x$. J is hopping strength which we choose as unity unless stated otherwise, and h is the strength of the transverse field. The spin chain is coupled with n number of isolated qubits for which the Hamiltonian is H_q and Σ_i denotes the Pauli matrix corresponding to i th qubit. The energy gap between the two lowest eigenstates for the isolated qubits is denoted by δ . κ is the strength of homogeneous interaction between a qubit and Ising spin while b represents the distance between consecutive isolated qubits. For the case $L = nb$, the complete Hamiltonian is translation invariant with a unit cell containing b Ising spins and one isolated qubit. For all the other cases, this symmetry is broken.

In addition to translation symmetry, the model has spin-flip symmetry, i.e. the Hamiltonian remains invariant when spin is flipped along x and y direction while keeping spin in z direction unchanged. The symmetry operator is given by,

$$P = \prod_{i=1}^L \sigma_i^z \otimes \prod_{j=1}^n \Sigma_j^z \quad (4)$$

which commutes with the Hamiltonian in Eq. 2 and satisfies $P^2 = I$. Therefore, Hamiltonian has a disjoint spectrum corresponding to $P = \pm 1$. For integrable to chaotic transition, spectral distribution is studied for a fixed symmetry sector, $P = +1$.

To show the generality of results obtained in subsequent sections, we also study a version of the sunburst quantum Ising model where we replace transverse field Ising ring by disordered XXZ spin chain and refer to it as the sunburst quantum XXZ model. The subsystem Hamiltonian is,

$$H_{XXZ} = \sum_{i=1}^L \sigma_i^x \sigma_{i+1}^x + \sigma_i^y \sigma_{i+1}^y + \sigma_i^z \sigma_{i+1}^z + W_i \sigma_i^z, \quad (5)$$

where W_i is a uniform random number distributed between $[-D, D]$ with D as disorder strength. The Hamiltonian shows a transition from ergodic to a many-body

localized (MBL) phase as the strength of the disorder is increased with the transition point at $D \approx 3.6$ [49–52]. Notice that the MBL phase presents a situation where the nearest neighbor spacings are Poisson distributed like the transverse Ising chain despite the lack of integrability in the traditional sense. Coupling this with isolated qubits through identical interaction terms, as given in Eq. 3, presents another example where two subsystems showing Poisson distributed spacing behavior, when coupled, lead to the Wigner-Dyson spacings, as shown in Fig. 1.

III. SPECTRAL FLUCTUATION: INTEGRABLE TO QUANTUM CHAOTIC TRANSITION

Spectral fluctuation properties such as spacing distribution have traditionally been used to classify dynamical systems. For generic integrable systems, nearest neighbor spacings follow Poisson distribution [53] while for systems with classically chaotic limits follow Wigner-Dyson statistics [54]. The nearest neighbor spacing distribution is between these two limits for a general non-integrable model. Calculating nearest neighbor spacing distribution requires eigenvalues unfolding, which is carried out numerically for most of the system. The sunburst quantum Ising model in the non-interacting limit is an integrable system. The integrability is broken in the presence of interaction terms between the Ising ring and qubits. To follow the complete integrable to chaotic transition as a function of coupling strength κ , we utilize the average ratio of the nearest neighbor spacing, which captures the statistical correlation in the same fashion as spacing distribution with the added advantage of relaxing the requirement of unfolding of spectrum [55, 56]. The ratio of nearest-neighbour spacing \tilde{r}_n is defined as

$$\tilde{r}_n = \frac{\min(s_n, s_{n-1})}{\max(s_n, s_{n-1})}; \quad s_n = E_{n+1} - E_n \quad (6)$$

where E_n is the n th eigenvalue. The ensemble-averaged ratio of spacing $\langle \tilde{r} \rangle$ takes the approximate value of 0.38 for the Poisson spectrum (integrable system) while for Gaussian Orthogonal Ensemble is approximately 0.53 (quantum chaotic systems with orthogonal symmetry)[55, 56]. The average ratio of spacing for the sunburst quantum Ising model initially increases almost linearly with increasing coupling strength κ then saturates around the value 0.53 (GOE) for $\kappa \gtrsim 0.5$, as seen in Fig. 1 (blue circles). Interestingly, for smaller coupling κ , $\langle \tilde{r} \rangle$ goes below Poisson value displaying the presence of Shnirelman’s peak [57–59]. Let us recall that according to Shnirelman’s theorem, for classically nearly integrable systems, at least every second spacing becomes exponentially small, causing a peak in spacing distribution at zero spacing [57, 58]. For the systems with no classical analog, this effect can be attributed to discrete symmetries, which generate the quasi-degenerate pair of eigenvalues. For very small κ , in the sunburst quantum Ising model

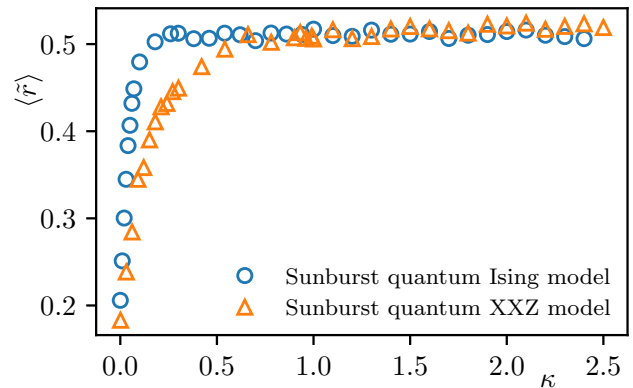


FIG. 1. We plot here $\langle \tilde{r} \rangle$ as a function of κ . For $\kappa \lesssim 0.1$, $\langle \tilde{r} \rangle$ is closer to the Poisson limit, which indicates the system is in the integrable regime. For $0.1 \lesssim \kappa \lesssim 0.5$, the system is in transition from integrable to the chaotic regime. For $0.5 \lesssim \kappa$, $\langle \tilde{r} \rangle$ is closer to the GOE limit, which indicates the system is in a chaotic regime. The system parameters are chosen as $\delta = 1$, to break the translational symmetry h_i s are taken as a uniformly distributed random number between 0.8 to 1, i.e. $h_i \in \text{Unif}[0.8, 1]$ along with $L = 9, n = 3$. For the XXZ chain $W_i \in \text{Unif}[-4, 4]$. The ensemble of 40 realizations is considered for both models.

as well as in the sunburst quantum XXZ model, the discrete permutation symmetry of interchanging qubits is almost a good symmetry responsible for enhanced values of smaller spacings. We have numerically verified that a small variation in δ_i removes this permutation symmetry and causes the disappearance of enhanced peak at zero spacing (figure not included). We show only a portion of the plot to clearly highlight the transition and plateauing. Utilizing this curve, we identify three regions (i) integrable ($\kappa \approx 0$), (ii) transition regime ($0.1 \lesssim \kappa \lesssim 0.5$), and (iii) chaotic limit ($\kappa \gtrsim 0.5$). (For a single qubit connected with the Ising core, see Appendix A.) For these three regions, the fate of an initial state turns out very different from each other. We probe the post-quench dynamics of an initial state using entanglement in Section IV.

IV. POST-QUENCH DYNAMICS: LINEAR ENTROPY

In this section, we seek to understand the role of coupling strength κ in generating the dynamics for the initial state, which is taken as product state of respective ground states of Ising ring and isolated qubits. Such a scenario is popularly known as out-of-equilibrium dynamics under sudden interaction quench. The quench protocol is,

$$H = \begin{cases} H_I \otimes \mathbb{1}_q + \mathbb{1}_I \otimes H_q & t < 0 \\ H_I \otimes \mathbb{1}_q + \mathbb{1}_I \otimes H_q + V_{Iq} & t \geq 0. \end{cases} \quad (7)$$

We use the linear entropy of the subsystem (qubits) as a probe to understand the out-of-equilibrium dynamics. Linear entropy of qubits is defined as

$$(S_L)_q = 1 - \text{tr}(\rho_q^2), \quad (8)$$

where ρ_q is the reduced density matrix of the qubits obtained by taking a partial trace over Ising degree of freedom. A note of caution here is that linear entropy is not a true measure of entanglement; rather, it measures the amount of mixedness of the subsystems, which increases with increasing the entanglement between the subsystems. As a result, linear entropy can roughly quantify the degree of entanglement between the subsystems [60]. In the limiting case of subsystems being in a pure state, linear entropy is zero. As we seek to characterize the nature of equilibration in the large time limit, we will focus on the time average and variance of linear entropy.

A. Limiting case: $h = 0, L > 1, n = 1$

To gain analytical insight, we derive an exact expression for linear entropy in the limiting case when we connect one qubit with the Ising ring and take $h = 0$. The ground state of transverse Ising model with $h = 0$, consistent with the \mathbb{Z}_2 symmetry, is $|\psi_G^I\rangle = \frac{1}{\sqrt{2}}[|++++\dots\rangle + |-----\rangle]$. This macroscopic superposition is known as the ‘‘cat state’’ [61], or GHZ state [62] in literature, and their generation has attracted much attention [63–66]. For non-zero but small h , this state is the true ground state of the transverse Ising chain. Although very fragile against ‘‘symmetry breaking’’ perturbation in $N \rightarrow \infty$ limit, this state is still interesting to study as our interaction term does not break the \mathbb{Z}_2 symmetry. The ground state of the pre-quench Hamiltonian is,

$$\begin{aligned} |\psi(0^-)\rangle &= |\psi_G^I\rangle \otimes |0\rangle, \text{ with} \\ |\psi_G^I\rangle &= \frac{1}{\sqrt{2}}[|++++\dots\rangle + |-----\rangle] \end{aligned} \quad (9)$$

with $\sigma_x |\pm\rangle = \pm |\pm\rangle, \Sigma_z |0\rangle = |0\rangle$. The superscript I signifies the Ising part. In $h = 0$ limit, Ising Hamiltonian commutes with qubit and interaction part of the Hamiltonian, and therefore the time-evolution operator can be factorized and written as,

$$U = \exp(-iH_I t) \exp[-it(H_q + V_{Iq})] = U_I U_{Iq} = U_{Iq} U_I.$$

As the initial state (Eq. 9) is an eigenstate of U_I , its action on $|\psi(0^-)\rangle$ produces only a global phase which we can ignore. We can evaluate $U_{Iq} |\psi(0^-)\rangle$ in close form by noticing that $(H_q + V_{Iq}) |\psi(0^-)\rangle = -\frac{\delta}{2} |\psi_G^I\rangle \otimes |0\rangle - \kappa |\psi_N^I\rangle \otimes |1\rangle$ and $(H_q + V_{Iq})^2 |\psi(0^-)\rangle = \frac{\omega^2}{4} |\psi(0^-)\rangle$ with

$\omega^2 = \delta^2 + 4\kappa^2$. The evolved state at any time t is,

$$\begin{aligned} |\psi(t)\rangle &= A(t) |\psi_G^I\rangle \otimes |0\rangle + B(t) |\psi_N^I\rangle \otimes |1\rangle, \\ |\psi_N^I\rangle &= \frac{1}{\sqrt{2}}[|++++\dots\rangle - |-----\rangle] \\ A(t) &= \cos \frac{\omega t}{2} + i \frac{\delta}{\omega} \sin \frac{\omega t}{2}, B(t) = \frac{2i\kappa}{\omega} \sin \frac{\omega t}{2}. \end{aligned} \quad (10)$$

The quench protocol produces a superposition of two eigenstates of pre-quench Hamiltonian that, interestingly, is already in Schmidt form. The reduced density matrix of the qubit is,

$$\rho_q(t) = \text{tr}_I(|\psi(t)\rangle \langle \psi(t)|) = |A(t)|^2 |0\rangle \langle 0| + |B(t)|^2 |1\rangle \langle 1|. \quad (11)$$

The linear entropy is then given by,

$$S_L(t) = 1 - (|A(t)|^4 + |B(t)|^4) \quad (12)$$

where $A(t), B(t)$ is defined in Eq. 10. It approaches to the maximum possible value when $|A(t)|^2 = |B(t)|^2 = \frac{1}{2}$. The time t^* when the linear entropy reaches its maximum is given by

$$t^* = \frac{2}{\omega} \cos^{-1} \left[\pm \sqrt{\frac{4\kappa^2 - \delta^2}{8\kappa^2}} \right]. \quad (13)$$

It is clear from Eq. 13 that linear entropy can reach its maximum possible limit only if the interaction strength κ is greater than or equal to half of the energy gap of the qubit i.e. $2\kappa \geq \delta$. If this condition is satisfied, t^* decreases with increasing κ , implying that the linear entropy reaches its maximum value faster for the larger interaction strength which is what we expect intuitively.

For small but non-zero h such that $h \ll J$, $|\psi_G^I\rangle, |\psi_N^I\rangle$ are no longer the exact eigenstate of the Ising ring, however, to a very good approximation, $|\psi(t)\rangle$ continues to be of the form given in Eq. 10. We compare the linear entropy calculated in Eq. 12 with exact diagonalization calculation for $h = 0.1, J = 1$ in Fig. 2. They are in good agreement.

B. Limiting case: $J = 0, L > 1, n = 1$

In this limit, the ground state of pre-quench Hamiltonian is given by,

$$|\psi(0^-)\rangle = |\psi_G^I\rangle \otimes |0\rangle, \text{ with } |\psi_G^I\rangle = |000\dots 0\rangle, \quad (14)$$

where $|\psi_G^I\rangle \otimes |0\rangle$ is the ground state of pre-quench Hamiltonian with ground state energy $E_G = -Lh - \frac{\delta}{2}$. The Ising Hamiltonian no longer commutes with V_{Iq} and therefore, the unitary evolution operator is given by $U = \exp(-it(H_I + H_q + V_{Iq}))$. In this limit $J = 0$, repeated application of H on the pre-quench state does not yield the Identity operator. We set up a difference equation for $H^n |\psi(0^-)\rangle$ in terms of the initial state $|\psi(0^-)\rangle$

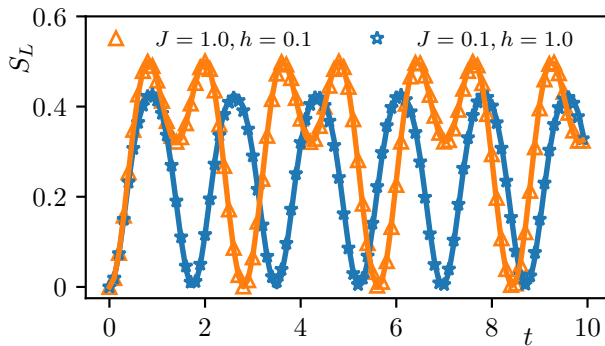


FIG. 2. In two limiting cases, the analytical expression of linear entropy is compared to the exact diagonalization calculations. In the weak field limit where $J = 1, h = 0.1, \delta = \kappa = 1$ numerics is shown by orange triangles while in the strong field limit where $J = 0.1, h = 1, \delta = \kappa = 1$ numerics is represented by blue stars. The respective analytical results (Eq. 12 with A, B given by Eq. 10 and 15 respectively) are plotted by solid lines. The period of the oscillation in both limits is $\frac{2\pi}{\omega}$.

and state $H|\psi(0^-)\rangle$ [67]. Solving this difference equation using the characteristic root method, we obtain the time-evolved state at the time t (see Appendix B for the details),

$$\begin{aligned} |\psi(t)\rangle &= A(t)|\psi_G^I\rangle \otimes |0\rangle + B(t)|\psi_N^I\rangle \otimes |1\rangle, \\ |\psi_N^I\rangle &= |100\dots 0\rangle \\ A(t) &= \cos\frac{\omega t}{2} + i\frac{\delta + 2h}{\omega}\sin\frac{\omega t}{2}, B(t) = \frac{2i\kappa}{\omega}\sin\frac{\omega t}{2}. \end{aligned} \quad (15)$$

Note $|\psi_N^I\rangle \otimes |1\rangle$ also is an eigenstate of pre-quench Hamiltonian with eigenvalue $E_N = -(L-2)h + \frac{\delta}{2}$. The expression for linear entropy, given in Eq. 12 is valid in this limiting case as well with modified $\omega^2 = (2h + \delta)^2 + 4\kappa^2$.

The oscillatory behavior of linear entropy clearly shows a lack of equilibration. Like the previous limit, for small but non-zero $J \ll h$, the expression of linear entropy matches very well with exact diagonalization calculation as $|\psi(t)\rangle$ continues to be a good approximation for finite but small J . The analytical expression and exact diagonalization result for parameters $J = 0.1, h = 1$ are compared in Fig. 2 and are in good agreement.

C. General case: $J = 1, h \approx \delta \approx \kappa \approx O(1), L > 1, n > 1$

For the parameter regime, $h \approx \delta \approx \kappa \approx O(1)$, the total system is in the chaotic regime (see Fig. 1). An analytical solution for the time evolution of the linear entropy is beyond this method. To understand the time evolution of linear entropy under interaction quench and bring out the role played by *coherence* of the initial state, we turn to exact diagonalization. In this case, linear entropy tends to saturate around a mean closer to the Lubkin value.

When the large time limit of linear entropy corresponds to the Lubkin value [47], we call such an equilibration thermalization.

In the rest of the paper, we try to understand perturbatively the initial growth of the linear entropy and, using this, whether or not a complete transition happens to a thermalized state. The emphasis will be on the role of initial coherence in the thermalization process characterized here by linear entropy. The exact diagonalization calculations for both models are done for system size $L = 9$ and $n = 1, 3$ along with $J = 1, h \approx 1$ unless mentioned otherwise.

V. ROLE OF INITIAL STATE COHERENCE IN POST-QUENCH DYNAMICS

The coherence of a state is a basis-dependent quantity, and we prefer to choose the energy basis to quantify the coherence. A state is called *incoherent* in the given basis set $\mathcal{B} = \{|m\rangle\}_{m=1}^N$ if the density matrix corresponding to this state is diagonal in the said basis. A deviation from this earns the name *coherent*. We use the sum of the square of off-diagonal elements of the density matrix ρ as coherence measure [68],

$$c_{\mathcal{B}}^2(\rho) = \sum_{m \neq m'} |\rho_{mm'}|^2.$$

A maximally coherent state in this basis is given by,

$$|\alpha_c\rangle = \frac{1}{\sqrt{N}} \sum_{m=1}^N e^{i\phi_m} |m\rangle \quad (16)$$

where $\phi_m \in \text{Unif}[0, 2\pi)$ and can be chosen randomly [69]. Recently, the role of coherence has been explored in the thermalization of the initial state using random matrix theory, where individual subsystems are modeled by random matrices [46]. It has been shown that the presence or lack of coherence in the initial state results in strong or weak thermalization. In this section, we first obtain perturbatively the very short time behavior of post-quench linear entropy for the initial state chosen as (a) the direct product of an incoherent state (ground state of the Ising ring and ground state of a single qubit), (b) the direct product of maximally coherent state constructed using all the eigenstates of the Ising ring with the ground state of a single qubit. By redefining the interaction strength, we can write down the result for many qubits using the conjecture proposed in [48]. Finally, we show that when time evolved by a strongly interacting sunburst quantum Ising model, the maximally coherent initial state thermalizes while the incoherent state continues to fluctuate about the long-time average value.

A. Short-time behaviour

Let us take the initial state of the sunburst quantum Ising ring with a single qubit as

$$|\psi(0^-)\rangle = |\alpha_c\rangle \otimes |0\rangle = \frac{1}{\sqrt{2^L}} \sum_{m=1}^{2^L} e^{i\phi_m} |\psi_m^I\rangle \otimes |0\rangle, \quad (17)$$

with $|\psi_m^I\rangle$ as m th eigenstates of the Ising ring and $\phi_m \in \text{Unif}[0, 2\pi)$ i.e., ϕ_m is chosen randomly for each m from uniform distribution as in Eq. 16. In the interaction picture, the time evolution operator can be approximated for a very short time ($t \ll \kappa^{-1}$) by $U_I(t) \approx \exp(-iV_{Iq}t)$ (for details see Appendix C). Time evolved state corresponding to the initial state given in Eq. 17 can be calculated using the series expansion of $\exp(-iV_{Iq}t)$ and re-summing the series after applying each term on the initial state. For applying V_{Iq} on the initial state, it is sensible to expand each of the eigenstates as a linear superposition of σ_z eigenbasis, i.e.

$$|\alpha_c\rangle = \frac{1}{\sqrt{2^L}} \sum_{m=1}^{2^L} e^{i\phi_m} \sum_{n=1}^{2^L} c_{nm} |n\rangle, \quad (18)$$

where $|n\rangle \in \{|00\dots 0\rangle, |00\dots 1\rangle, \dots |11\dots 1\rangle\}$.

The action of V_{Iq} once on initial state will produce, the state $|\alpha'_c\rangle \otimes |1\rangle$ with,

$$|\alpha'_c\rangle = \frac{1}{\sqrt{2^L}} \sum_{m=1}^{2^L} e^{i\phi_m} \sum_{n=1}^{2^L} c_{nm} |\tilde{n}\rangle, \quad \text{where } |\tilde{n}\rangle = \sigma_1^x |n\rangle. \quad (19)$$

Applying V_{Iq} twice on the initial state will return the initial state as is evident from Eq. 18, 19. This helps in obtaining a closed-form expression for $|\psi(t)\rangle$ as

$$|\psi(t)\rangle = \cos(\kappa t) |\alpha_c\rangle \otimes |0\rangle + i \sin(\kappa t) |\alpha'_c\rangle \otimes |1\rangle. \quad (20)$$

The subsystem linear entropy at time t is,

$$S_L = \frac{1}{4} [1 - \cos(4\kappa t)] [1 - |\gamma|^2] \quad (21)$$

where

$$\gamma = \langle \alpha_c | \alpha'_c \rangle. \quad (22)$$

Depending on the initial coherence, γ changes. Let us take the extreme case when $N = 1$ i.e. only the ground state of the Ising ring is taken, which is an example of *incoherent* initial state. Note that $|\alpha'_c\rangle$ is orthogonal to $|\alpha_c\rangle$ in this case, and therefore $\gamma = 0$. The fact that parity commutes with the Ising Hamiltonian and anti-commutes with interaction, results in the orthogonality of $|\alpha_c\rangle$ and $|\alpha'_c\rangle$. The linear entropy for an incoherent initial state then becomes,

$$S_L = \frac{1}{4} (1 - \cos(4\kappa t)), \quad (23)$$

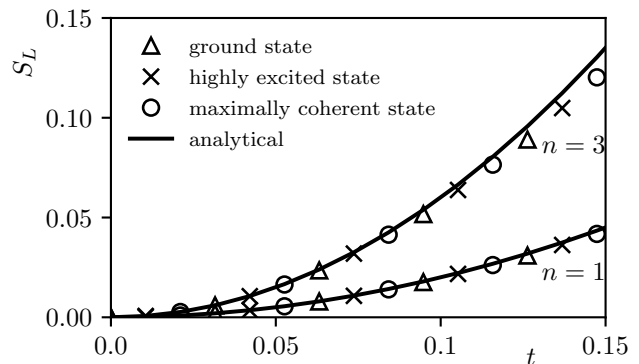


FIG. 3. Initial growth of linear entropy is plotted for different initial states, such as two incoherent states constructed from (a) the ground state (\triangle) of the Ising ring, (b) a state from the middle of the spectrum of the Ising ring (\times) and the maximally coherent state (\circ) as a function of time. The length of the Ising ring is taken as $L = 9$ for all the sets while the number of qubits is taken as $n = 1$ and 3 . The solid line for $n = 1$ is the quadratic curve derived in Eq. 24, while for $n = 3$ denotes the Eq. 25. The other system parameters are $h = 0.95, \delta = 1, \kappa = 1$. The quadratic behavior of linear entropy for a short time is clearly visible for all the initial states.

which, for a very short time,

$$S_L \approx 2\kappa^2 t^2. \quad (24)$$

This quadratic dependence on time is a clear departure from earlier studied linear dependence of linear entropy on time [70–74]. A maximal coherent state with random phases can be expanded in σ_z eigenbasis with random coefficients as given in Eq. 18. The action of V_{Iq} on this will produce another unit vector with random coefficients as defined in Eq. 19. For maximally coherent state, we approximate $|\alpha_c\rangle, |\alpha'_c\rangle$ by two independent random unit vectors and as $|\gamma|$ is defined as the dot product of these two random vectors, average of $|\gamma|^2$ over the random phases is equal to the variance of the dot product of two unit random vectors which is of the order of $1/2^L$ [75?]. To check the approximation of taking $|\alpha_c\rangle, |\alpha'_c\rangle$ as random vectors in σ_z eigenbasis, we have numerically checked that average of $|\gamma|^2$ over random phases scales as $1/2^L$ (figure not shown here). This contribution vanishes in a large L limit. Let us recall again that this behavior applies to a very short time during which the interaction propagator is written in terms of only V_{Iq} .

For the Ising ring coupled with two qubits, the short-time behavior of the linear entropy continues to be quadratic, specifically as $S_L \approx 4\kappa^2 t^2$ (for details see Appendix D). This result is in agreement with the scaling conjecture numerically verified in [48]. Motivated by this, for the Ising ring connected with n -qubits, the growth of linear entropy is taken as,

$$S_L \approx 2n\kappa^2 t^2. \quad (25)$$

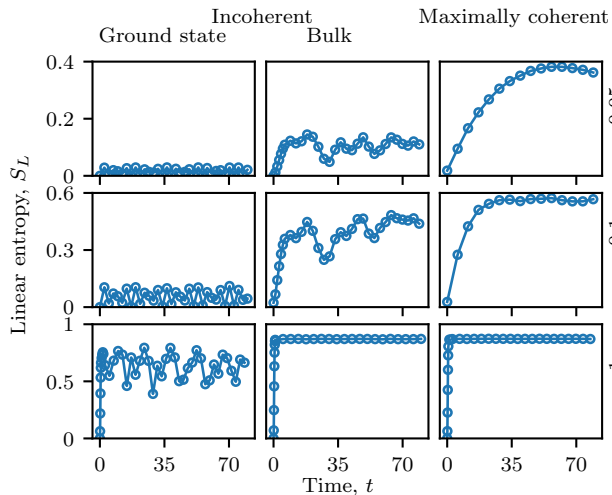


FIG. 4. Time variation of linear entropy for incoherent and maximally coherent initial state in ultra-weak ($\kappa = 0.05$), weak ($\kappa = 0.1$) and strong interaction ($\kappa = 1$) regimes. We have considered $L = 9$, $n = 3$ and $J = \delta = 1$, $h = 0.95$.

This conjecture agrees very well with exact diagonalization calculations as seen in Fig. 3 where the length of the Ising ring is $L = 9$ and the number of qubits is $n = 3$.

B. Long time averaged entropy

Not surprisingly, when we time evolve the direct product of the ground state of the Ising ring with the ground state of non-interacting qubits (*i.e.* incoherent state) by near-integrable quenched Hamiltonian ($\kappa = 0.05$), the linear entropy fluctuates a lot near zero value (see Fig. 4). For a larger value of interaction strength ($\kappa = 1$) when quenched Hamiltonian has a spectrum with Wigner-Dyson spacing, the time-averaged linear entropy approaches the Lubkin value (random vector value) with visible fluctuations around it (see Fig. 4). In the second column of Fig. 4, we have shown the entanglement generation in an incoherent state which is a direct product of the eigenstate from the middle of the spectrum of the Ising Hamiltonian and the ground state of non-interacting qubits. The entanglement generated by the near-integrable case is more than the incoherent state corresponding to the ground state but less than the maximally coherent initial state. Only in the case of large $\kappa (= 1)$, the entanglement generation is the same as in the case of a maximal coherent state.

On the other hand, we have plotted linear entropy with time in the third column when the initial state is taken as a maximally coherent state and evolved in time with the quenched Hamiltonian of the same coupling strength as in the first and second columns of Fig. 4. It is clear that the magnitude of fluctuations is significantly lower compared to the incoherent initial state counterparts as

well as more entanglement has been generated in case of $\kappa = 0.05, 0.1$. Infinite time-averaged entropy and variance to capture temporal fluctuation around it are defined as,

$$\langle S_L \rangle = \lim_{\tau \rightarrow \infty} \frac{1}{\tau} \int_0^\tau S_L(t) dt, \quad (26)$$

$$\sigma^2(S_L) = \langle (S_L(t) - \langle S_L \rangle)^2 \rangle.$$

We have tabulated the effect of coherence on the long-time averaged value of entropy along with variance to quantify this fluctuation in Tab. I.

	$L = 9, n = 1$	$L = 9, n = 3$		
$c_{\mathcal{B}}^2$	$\langle S_L(t) \rangle$	$\sigma^2(S_L)$	$\langle S_L(t) \rangle$	$\sigma^2(S_L)$
0.5000	0.2309	0.1103	0.5704	0.0651
0.7500	0.3236	0.0766	0.6959	0.0488
0.8750	0.3634	0.0635	0.7587	0.0247
0.9375	0.4100	0.0393	0.7849	0.0147
0.9687	0.4217	0.0286	0.8227	0.0082
0.9844	0.4651	0.0152	0.8408	0.0058
0.9922	0.4782	0.0090	0.8560	0.0030
0.9960	0.4877	0.0061	0.8654	0.0013
0.9980	0.4974	0.0018	0.8722	0.0005

TABLE I. The time-averaged entropy and variance is listed as a function of initial state coherence.

The variance decreases almost inversely proportional to the initial state coherence and, at the same time, the long-time averaged linear entropy increases to its limit of Lubkin value. This shows that coherence of the initial state acts as a resource for entanglement generation and decreasing variance signify strong thermalization.

To understand the possible mechanism of fluctuations in linear entropy around Lubkin value seen when an incoherent state is evolved in time with strongly coupled quenched Hamiltonian, we plot the inverse participation ratio (IPR) of the time-evolved state in the pre-quench eigenenergy basis. We define IPR as,

$$I_{|\psi(t)\rangle} = \sum_{m=1}^N |\langle \psi_m^{H_0} | \psi(t) \rangle|^4, \quad \text{with}$$

$$(H_I \otimes \mathbb{1}_q + \mathbb{1}_I \otimes H_q) |\psi_m^{H_0}\rangle = E_m |\psi_m^{H_0}\rangle, m = 1 \dots N. \quad (27)$$

This quantity takes two extreme values: 1 and $1/N$ (inverse of Hilbert space dimension) for the limits when the time-evolved state is built upon only one of the pre-quench states, and when it is built upon all the pre-quench eigenstates, respectively. To show the correlation, we have plotted $\tilde{I}(t) \equiv 1 - I_{|\psi(t)\rangle}$ (red dashed line for $n = 1$ qubit, and green dotted lines for $n = 3$ qubits) along with linear entropy (blue star for $n = 1$ qubit and orange circle for $n = 3$ qubits) as seen in Fig. 5. For $n = 1$ qubit, $\tilde{I}(t)$ is fluctuating and averaging to nearly half. This shows that the time-evolving state explores

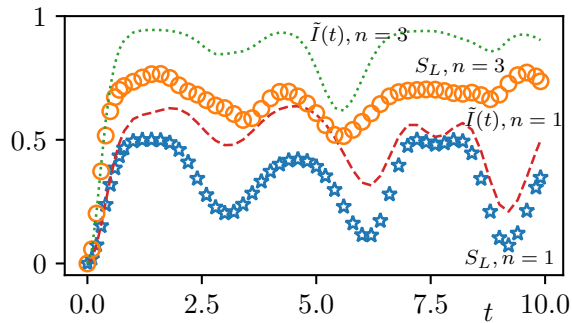


FIG. 5. Time evolution of linear entropy and $\tilde{I}(t)$ of the state $|\psi(t)\rangle$ evolved in time by post-quench sunburst quantum Ising Hamiltonian are plotted here. The blue star and orange circle are linear entropy for the sunburst quantum Ising model for $n = 1$ and $n = 3$ qubits, respectively. Red dashed line ($n = 1$ qubits) and green dotted line ($n = 3$ qubits) are representing $\tilde{I}(t)$ for the same time evolved state in pre-quench eigenbasis. For these $\kappa = \delta = 1.0$ has been taken along with $h = 0.95$, and the initial state is incoherent. The choice of plotting $\tilde{I}(t)$ in place of $I_{|\psi(t)\rangle}$ is to show the hills and valleys correspond exactly to those of linear entropy.

a very small subset of Hilbert space of the pre-quench system, and therefore we see a large fluctuation in entropy. This fact is borne out in the Fig. 5 very clearly where the smaller value of IPR (i.e., a larger value of $\tilde{I}(t)$ as plotted in the figure) corresponds to larger entanglement entropy. This clearly shows that an increase (decrease) in entanglement entropy corresponds to instantaneous larger (smaller) participation of pre-quench eigenstates in the time-evolved incoherent initial state. For the maximally coherent initial state (Eq. 17) on the other hand, IPR calculated in the pre-quench eigenenergy basis is approximately independent of time. This observation is intuitively clear as a maximally coherent state is constructed with all eigenstates of the Ising ring. The IPR comes out to be $\approx 1/2^{L+n}$, which shows that the complete Hilbert space of the pre-quench Hamiltonian is explored by the time-evolving state for all time.

For the case when complete Hilbert space is being explored, we derived the initial dependence of linear entropy on time to be quadratic (Eq. 24). Using the perturbation theory developed in [39] and initial time dependence of entropy, the complete transition of linear entropy from 0 to Lubkin value can be obtained (see Appendix E),

$$S_L(t) = \left[1 - \exp\left(-\frac{2\kappa^2 t^2}{S_L^\infty}\right) \right] S_L^\infty. \quad (28)$$

This form is compared with linear entropy calculated numerically for sunburst quantum Ising model when a single qubit is connected with the Ising ring in Fig. 6 (orange circles). Utilizing the initial time-dependence of entropy for the sunburst quantum Ising model with n -qubits,

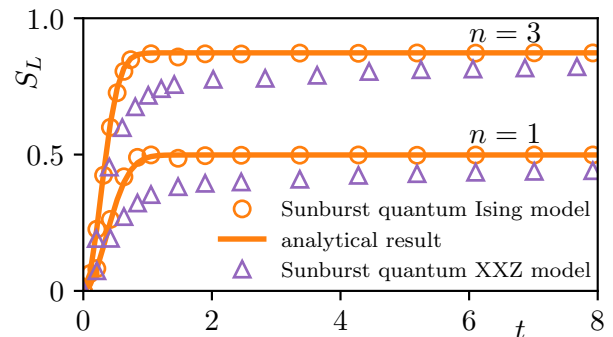


FIG. 6. Evolution of linear entropy when maximally coherent product state is evolved by the sunburst quantum Ising model and sunburst quantum XXZ model. In the XXZ model, parameters are chosen in such a way that the system is in the MBL phase. The solid lines are analytical results derived in Eqs. 28, 29. The sunburst quantum XXZ model where qubits are connected with the ring of XXZ chain with disorder strength $D = 4$ puts the XXZ ring in the many-body localized phase. The other parameters are $\delta = 1$, $L = 9$, and $\kappa = 1.5$.

Eq. 28 is generalized to,

$$S_L(t) = \left[1 - \exp\left(-\frac{2n\kappa^2 t^2}{S_L^\infty}\right) \right] S_L^\infty. \quad (29)$$

This result is in clear agreement with the exact diagonalization calculation as seen in Fig. 6 where $n = 3$ qubits have been chosen (orange circles), and like in the single qubit case, the initial condition was a maximally coherent state.

For both cases, whether the initial state is incoherent or maximally coherent, the reduced density matrix corresponding to the qubit subspace becomes nearly diagonal, a telltale sign of equilibration. The fluctuation in linear entropy then captures whether equilibration is strong or weak. Therefore, the variance of the time series of linear entropy becomes a good measure to identify the nature of the equilibration of the time-evolved state. As seen in Table. I, for a fixed coupling strength where the total system is quantum chaotic, and variance is (almost) inversely proportional to the degree of coherence of the initial state. The time-averaged value of linear entropy becoming equal to the Lubkin value with a very small variance indicates the strong thermalization when the initial state is maximally coherent and time-evolution is done using post-quench Hamiltonian showing Wigner-Dyson statistics for its spectral fluctuation. On the other hand, thermalization remains weak for an incoherent initial state for the same value of coupling constant κ .

For the sunburst quantum XXZ model, the average ratio of spacing with coupling strength κ is plotted in Fig. 1 (orange triangle), showing a transition from integrability to chaos. We choose a sufficiently large κ value to correspond to the average ratio of the spacings

to correspond to Wigner-Dyson statistics. The time evolution of linear entropy of qubits post interaction quench in the sunburst quantum XXZ model is plotted in Fig. 6. The numerical linear entropy evolution closely follows the analytical form derived for the sunburst quantum Ising model, as is borne out clearly from Fig. 6. A systematic lower value of linear entropy from the Lubkin value may be specific to MBL physics, which we will take up for a future study.

VI. SUMMARY AND OUTLOOK

In this paper, we have studied the non-equilibrium dynamics of an isolated bipartite quantum system, the sunburst quantum Ising model, under interaction quench where pre-quench subsystems are integrable. The interaction strength drives the post-quench system to a quantum chaotic regime, with the average ratio of spacings being ≈ 0.53 for $\kappa \gtrsim 0.5$ consistent with GOE of random matrix theory. We have derived a quadratic in time growth of linear entropy for short time. The coherence of the initial state is shown to slow it down a little, but the contribution is vanishingly small as we increase the length of the Ising ring. The initial state, which we chose as a product state of eigenstates of pre-quench Hamiltonian subsystems, equilibrates in the large time limit when

the post-quench Hamiltonian generates the time evolution with interaction strength value one or larger as long as level spacing distribution remains Wigner-Dyson. We derived the full transition curve for linear entropy, which agrees with numerical calculation. We further highlight the increase in time-averaged entropy (Eq. 26) tabulated in Tab. 1 as a function of the initial state coherence, suggestive of later being a resource of entanglement. The decreasing variance of linear entropy with initial state coherence characterizes the smallness of oscillations around the mean value, or in other words, initial state coherence helps in achieving the steady state behavior even in a weak interaction regime (see the second row of Fig. 4). We have shown that the effect of coherence on the nature of equilibrium is a “generic” feature of bipartite near-integrable/quantum chaotic systems with individual parts taken as integrable by replacing the Ising ring with XXZ chain taken in the MBL phase. Though quantifying this effect analytically has earlier been done using random matrix theory in the limit when pre-quench subsystems are chaotic [46], it remains an open problem for integrable subsystems as studied here. The lack of sunburst quantum XXZ model (in MBL phase) in attaining the Lubkin value for linear entropy despite the overall system showing Wigner-Dyson spacing also remains an interesting open question to explore.

-
- [1] T. Kinoshita, T. Wenger, and D. Weiss, A quantum newton’s cradle, *Nature* **440**, 900 (2006).
 - [2] M. Cheneau, P. Barmettler, D. Poletti, M. Endres, P. Schauß, T. Fukuhara, C. Gross, I. Bloch, C. Kollath, and S. Kuhr, Light-cone-like spreading of correlations in a quantum many-body system, *Nature* **481**, 484 (2012).
 - [3] T. Langen, S. Erne, R. Geiger, B. Rauer, T. Schweigler, M. Kuhnert, W. Rohringer, I. E. Mazets, T. Gasenzer, and J. Schmiedmayer, Experimental observation of a generalized gibbs ensemble, *Science* **348**, 207 (2015).
 - [4] T. Brydges, A. Elben, P. Jurcevic, B. Vermersch, C. Maier, B. P. Lanyon, P. Zoller, R. Blatt, and C. F. Roos, Probing rényi entanglement entropy via randomized measurements, *Science* **364**, 260 (2019).
 - [5] A. Lukin, M. Rispoli, R. Schittko, M. E. Tai, A. M. Kaufman, S. Choi, V. Khemani, J. Léonard, and M. Greiner, Probing entanglement in a many-body-localized system, *Science* **364**, 256 (2019).
 - [6] U. Schneider, L. Hackermüller, J. P. Ronzheimer, S. Will, S. Braun, T. Best, I. Bloch, E. Demler, S. Mandt, D. Rasch, and A. Rosch, Fermionic transport and out-of-equilibrium dynamics in a homogeneous hubbard model with ultracold atoms, *Nature Physics* **8**, 213 (2012).
 - [7] M. Gring, M. Kuhnert, T. Langen, T. Kitagawa, B. Rauer, M. Schreitl, I. Mazets, D. A. Smith, E. Demler, and J. Schmiedmayer, Relaxation and prethermalization in an isolated quantum system, *Science* **337**, 1318 (2012).
 - [8] A. M. Kaufman, M. E. Tai, A. Lukin, M. Rispoli, R. Schittko, P. M. Preiss, and M. Greiner, Quantum thermalization through entanglement in an isolated many-body system, *Science* **353**, 794 (2016).
 - [9] S. Trotzky, Y.-A. Chen, A. Flesch, I. P. McCulloch, U. Schollwöck, J. Eisert, and I. Bloch, Probing the relaxation towards equilibrium in an isolated strongly correlated one-dimensional bose gas, *Nature Physics* **8**, 325 (2012).
 - [10] T. Langen, R. Geiger, M. Kuhnert, B. Rauer, and J. Schmiedmayer, Local emergence of thermal correlations in an isolated quantum many-body system, *Nature Physics* **9**, 640 (2013).
 - [11] R. Islam, R. Ma, P. M. Preiss, M. Eric Tai, A. Lukin, M. Rispoli, and M. Greiner, Measuring entanglement entropy in a quantum many-body system, *Nature* **528**, 77 (2015).
 - [12] S. Ritter, A. Öttl, T. Donner, T. Bourdel, M. Köhl, and T. Esslinger, Observing the formation of long-range order during bose-einstein condensation, *Phys. Rev. Lett.* **98**, 090402 (2007).
 - [13] J. M. Deutsch, Quantum statistical mechanics in a closed system, *Phys. Rev. A* **43**, 2046 (1991).
 - [14] M. Srednicki, Chaos and quantum thermalization, *Phys. Rev. E* **50**, 888 (1994).
 - [15] J. M. Deutsch, Eigenstate thermalization hypothesis, *Reports on Progress in Physics* **81**, 082001 (2018).
 - [16] M. Rigol, V. Dunjko, and M. Olshanii, Thermalization and its mechanism for generic isolated quantum systems, *Nature* **452**, 854 (2008).
 - [17] M. Rigol and M. Srednicki, Alternatives to eigenstate thermalization, *Phys. Rev. Lett.* **108**, 110601 (2012).

- [18] L. D'Alessio, Y. Kafri, A. Polkovnikov, and M. Rigol, From quantum chaos and eigenstate thermalization to statistical mechanics and thermodynamics, *Advances in Physics* **65**, 239 (2016).
- [19] L. F. Santos and M. Rigol, Localization and the effects of symmetries in the thermalization properties of one-dimensional quantum systems, *Phys. Rev. E* **82**, 031130 (2010).
- [20] E. J. Torres-Herrera and L. F. Santos, Effects of the interplay between initial state and hamiltonian on the thermalization of isolated quantum many-body systems, *Phys. Rev. E* **88**, 042121 (2013).
- [21] R. Nandkishore and D. A. Huse, Many-body localization and thermalization in quantum statistical mechanics, *Annual Review of Condensed Matter Physics* **6**, 15 (2015), <https://doi.org/10.1146/annurev-conmatphys-031214-014726>.
- [22] F. Alet and N. Laflorencie, Many-body localization: An introduction and selected topics, *Comptes Rendus Physique* **19**, 498 (2018), quantum simulation / Simulation quantique.
- [23] D. A. Abanin, E. Altman, I. Bloch, and M. Serbyn, Colloquium: Many-body localization, thermalization, and entanglement, *Rev. Mod. Phys.* **91**, 021001 (2019).
- [24] H. Bernien, S. Schwartz, A. Keesling, H. Levine, A. Omran, H. Pichler, S. Choi, A. S. Zibrov, M. Endres, M. Greiner, V. Vuletić, and M. D. Lukin, Probing many-body dynamics on a 51-atom quantum simulator, *Nature* **551**, 579 (2017).
- [25] D. Bluvstein, A. Omran, H. Levine, A. Keesling, G. Semeghini, S. Ebadi, T. T. Wang, A. A. Michailidis, N. Maskara, W. W. Ho, S. Choi, M. Serbyn, M. Greiner, V. Vuletić, and M. D. Lukin, Controlling quantum many-body dynamics in driven rydberg atom arrays, *Science* **371**, 1355 (2021), <https://www.science.org/doi/pdf/10.1126/science.abg2530>.
- [26] P. Calabrese and J. Cardy, Evolution of entanglement entropy in one-dimensional systems, *Journal of Statistical Mechanics: Theory and Experiment* **2005**, P04010 (2005).
- [27] P. Calabrese and J. Cardy, Quantum quenches in 1+1 dimensional conformal field theories, *Journal of Statistical Mechanics: Theory and Experiment* **2016**, 064003 (2016).
- [28] V. Eisler and I. Peschel, Entanglement in a periodic quench, *Annalen der Physik* **520**, 410 (2008).
- [29] V. Alba, Entanglement and quantum transport in integrable systems, *Phys. Rev. B* **97**, 245135 (2018).
- [30] G. D. Chiara, S. Montangero, P. Calabrese, and R. Fazio, Entanglement entropy dynamics of heisenberg chains, *Journal of Statistical Mechanics: Theory and Experiment* **2006**, P03001 (2006).
- [31] P. Calabrese, Entanglement spreading in non-equilibrium integrable systems, *SciPost Physics Lecture Notes* **10.21468/scipostphyslectnotes.20** (2020).
- [32] M. Fagotti and P. Calabrese, Evolution of entanglement entropy following a quantum quench: Analytic results for the xy chain in a transverse magnetic field, *Phys. Rev. A* **78**, 010306(R) (2008).
- [33] M. G. Nezhadhighi and M. A. Rajabpour, Entanglement dynamics in short- and long-range harmonic oscillators, *Phys. Rev. B* **90**, 205438 (2014).
- [34] A. Coser, E. Tonni, and P. Calabrese, Entanglement negativity after a global quantum quench, *Journal of Statistical Mechanics: Theory and Experiment* **2014**, P12017 (2014).
- [35] A. S. Buyskikh, M. Fagotti, J. Schachenmayer, F. Essler, and A. J. Daley, Entanglement growth and correlation spreading with variable-range interactions in spin and fermionic tunneling models, *Phys. Rev. A* **93**, 053620 (2016).
- [36] J. Kudler-Flam, Y. Kusuki, and S. Ryu, The quasi-particle picture and its breakdown after local quenches: mutual information, negativity, and reflected entropy, *Journal of High Energy Physics* **2021**, 10.1007/jhep03(2021)146 (2021).
- [37] V. Alba and P. Calabrese, Entanglement and thermodynamics after a quantum quench in integrable systems, *Proceedings of the National Academy of Sciences* **114**, 7947 (2017).
- [38] V. Alba, B. Bertini, M. Fagotti, L. Piroli, and P. Ruggiero, Generalized-hydrodynamic approach to inhomogeneous quenches: correlations, entanglement and quantum effects, *Journal of Statistical Mechanics: Theory and Experiment* **2021**, 114004 (2021).
- [39] A. Lakshminarayan, S. C. L. Srivastava, R. Ketzmerick, A. Bäcker, and S. Tomsovic, Entanglement and localization transitions in eigenstates of interacting chaotic systems, *Phys. Rev. E* **94**, 010205(R) (2016).
- [40] A. Lakshminarayan, Entangling power of quantized chaotic systems, *Phys. Rev. E* **64**, 036207 (2001).
- [41] J. N. Bandyopadhyay and A. Lakshminarayan, Testing statistical bounds on entanglement using quantum chaos, *Phys. Rev. Lett.* **89**, 060402 (2002).
- [42] H. Fujisaki, A. Tanaka, and T. Miyadera, Dynamical aspects of quantum entanglement for coupled mapping systems, *Journal of the Physical Society of Japan* **72**, 111 (2003).
- [43] S. C. L. Srivastava, S. Tomsovic, A. Lakshminarayan, R. Ketzmerick, and A. Bäcker, Universal scaling of spectral fluctuation transitions for interacting chaotic systems, *Phys. Rev. Lett.* **116**, 054101 (2016).
- [44] S. Tomsovic, A. Lakshminarayan, S. C. L. Srivastava, and A. Bäcker, Eigenstate entanglement between quantum chaotic subsystems: Universal transitions and power laws in the entanglement spectrum, *Phys. Rev. E* **98**, 032209 (2018).
- [45] J. J. Pulikkottil, A. Lakshminarayan, S. C. L. Srivastava, A. Bäcker, and S. Tomsovic, Entanglement production by interaction quenches of quantum chaotic subsystems, *Phys. Rev. E* **101**, 032212 (2020).
- [46] J. J. Pulikkottil, A. Lakshminarayan, S. C. L. Srivastava, M. F. I. Kieler, A. Bäcker, and S. Tomsovic, Quantum coherence controls the nature of equilibration and thermalization in coupled chaotic systems, *Phys. Rev. E* **107**, 024124 (2023).
- [47] E. Lubkin, Entropy of an n-system from its correlation with a k-reservoir, *Journal of Mathematical Physics* **19**, 1028 (1978).
- [48] A. Franchi, D. Rossini, and E. Vicari, Quantum many-body spin rings coupled to ancillary spins: The sunburst quantum ising model, *Phys. Rev. E* **105**, 054111 (2022).
- [49] A. Pal and D. A. Huse, Many-body localization phase transition, *Phys. Rev. B* **82**, 174411 (2010).
- [50] D. J. Luitz, N. Laflorencie, and F. Alet, Many-body localization edge in the random-field heisenberg chain, *Phys. Rev. B* **91**, 081103(R) (2015).

- [51] M. Serbyn, Z. Papić, and D. A. Abanin, Criterion for many-body localization-delocalization phase transition, *Phys. Rev. X* **5**, 041047 (2015).
- [52] S. Bera and A. Lakshminarayan, Local entanglement structure across a many-body localization transition, *Phys. Rev. B* **93**, 134204 (2016).
- [53] M. V. Berry and M. Tabor, Level clustering in the regular spectrum, *Proc. R. Soc. A* **356**, 375 (1977).
- [54] O. Bohigas, M.-J. Giannoni, and C. Schmit, Characterization of chaotic quantum spectra and universality of level fluctuation laws, *Physical Review Letters* **52**, 1 (1984).
- [55] V. Oganesyan and D. A. Huse, Localization of interacting fermions at high temperature, *Phys. Rev. B* **75**, 155111 (2007).
- [56] Y. Y. Atas, E. Bogomolny, O. Giraud, and G. Roux, Distribution of the ratio of consecutive level spacings in random matrix ensembles, *Phys. Rev. Lett.* **110**, 084101 (2013).
- [57] A. I. Shnirelman, On asymptotic multiplicity of spectrum of laplace operator, *Usp. Mat. Nauk* **30**, 265 (1975).
- [58] A. I. Shnirelman, Addendum on the asymptotic properties of eigenfunctions in the regions of chaotic motion, in *KAM Theory and Semiclassical Approximations to Eigenfunctions* (Springer Berlin Heidelberg, Berlin, Heidelberg, 1993) pp. 313–337.
- [59] B. V. Chirikov and D. L. Shepelyansky, Shnirelman peak in level spacing statistics, *Phys. Rev. Lett.* **74**, 518 (1995).
- [60] J. N. Bandyopadhyay and A. Lakshminarayan, Entanglement production in quantized chaotic systems, *Pramana* **64**, 577 (2005).
- [61] E. Schrödinger, Die gegenwärtige situation in der quantenmechanik, *Naturwissenschaften* **23**, 823 (1935).
- [62] D. M. Greenberger, M. A. Horne, and A. Zeilinger, Going beyond bell’s theorem (2007), [arXiv:0712.0921](https://arxiv.org/abs/0712.0921) [quant-ph].
- [63] D. Bouwmeester, J.-W. Pan, M. Daniell, H. Weinfurter, and A. Zeilinger, Observation of three-photon greenberger-horne-zeilinger entanglement, *Phys. Rev. Lett.* **82**, 1345 (1999).
- [64] X. Wang, A. Bayat, S. Bose, and S. G. Schirmer, Global control methods for greenberger-horne-zeilinger-state generation on a one-dimensional ising chain, *Phys. Rev. A* **82**, 012330 (2010).
- [65] Y. Ji, J. Bian, X. Chen, J. Li, X. Nie, H. Zhou, and X. Peng, Experimental preparation of greenberger-horne-zeilinger states in an ising spin model by partially suppressing the nonadiabatic transitions, *Phys. Rev. A* **99**, 032323 (2019).
- [66] J. Li, G. R. M. da Silva, S. Kain, and S. M. Shahriar, Rapid generation of a macroscopic schrödinger cat state of atoms with parity-independent orientation (2022), [arXiv:2210.15115](https://arxiv.org/abs/2210.15115) [quant-ph].
- [67] X. Zhou, Q.-K. Wan, and X.-H. Wang, Many-body dynamics and decoherence of the xxz central spin model in external magnetic field, *Entropy* **22**, 10.3390/e22010023 (2020).
- [68] T. Baumgratz, M. Cramer, and M. B. Plenio, Quantifying coherence, *Phys. Rev. Lett.* **113**, 140401 (2014).
- [69] Y. Peng, Y. Jiang, and H. Fan, Maximally coherent states and coherence-preserving operations, *Phys. Rev. A* **93**, 032326 (2016).
- [70] A. Tanaka, H. Fujisaki, and T. Miyadera, Saturation of the production of quantum entanglement between weakly coupled mapping systems in a strongly chaotic region, *Phys. Rev. E* **66**, 045201 (2002).
- [71] J. N. Bandyopadhyay and A. Lakshminarayan, Entanglement production in coupled chaotic systems: Case of the kicked tops, *Phys. Rev. E* **69**, 016201 (2004).
- [72] P. Calabrese and J. Cardy, Evolution of entanglement entropy in one-dimensional systems, *Journal of Statistical Mechanics: Theory and Experiment* **2005**, P04010 (2005).
- [73] H. Kim and D. A. Huse, Ballistic spreading of entanglement in a diffusive nonintegrable system, *Phys. Rev. Lett.* **111**, 127205 (2013).
- [74] A. M. Kaufman, M. E. Tai, A. Lukin, M. Rispoli, R. Schittko, P. M. Preiss, and M. Greiner, Quantum thermalization through entanglement in an isolated many-body system, *Science* **353**, 794 (2016).
- [75] A. Kushkuley, A remark on random vectors and irreducible representations (2022), [arXiv:2110.15504](https://arxiv.org/abs/2110.15504) [math.PR].
- [76] H. F. Baker, Alternants and continuous groups, *Proceedings of the London Mathematical Society* **s2-3**, 24 (1905).
- [77] J. E. Campbell, On a law of combination of operators (second paper), *Proceedings of the London Mathematical Society* **1**, 14 (1897).
- [78] F. Hausdorff, Die symbolische exponentialformel in der gruppentheorie, *Ber. Verh. Kgl. Sächsisch. Ges. Wiss. Leipzig., Math.-phys. Kl.* **58**, 19 (1906).

Appendix A: Transition of the average ratio of spacing in sunburst quantum Ising model with $n = 1$

In this appendix, we present the behaviour of the average ratio of the spacing with increasing interaction strength in the sunburst quantum Ising model. In the

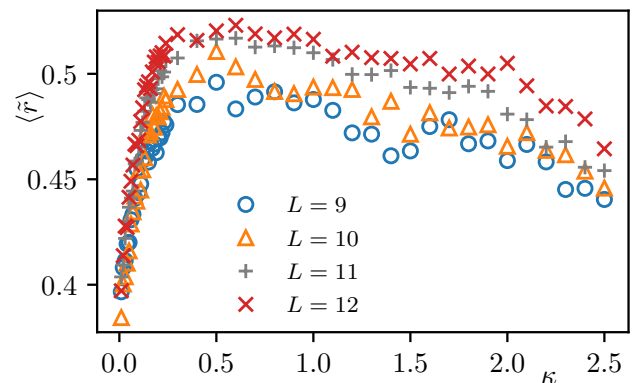


FIG. 7. Plot of $\langle \tilde{r} \rangle$ as a function of interaction strength κ for sunburst quantum Ising model for different values of L . The other parameters of the system are, $n = 1, J = \delta = 1, h \in \text{Unif}[0.8, 1)$.

$n = 1$ limit, the discrete permutation symmetry of interchanging qubits is no longer applicable therefore Shnirelman’s peak disappears and the average ratio of

spacing starts from ≈ 0.38 corresponding to the Integrable limit. For small L (say 9) and one qubit system, the average ratio of spacing never attains the GOE value of 0.53 signifying a lack of maximally quantum chaotic behaviour, however, with increasing L even with $n = 1$, the average ratio of spacing nearly reaches to GOE value and plateauing becomes more pronounced as seen in Fig. 7.

Appendix B: Evolution in $J = 0$ limit: solution using difference equation

In the $J = 0$ limit, the initial state is given by Eq. 14. The action of Hamiltonian given in Eq. 2 with $J = 0$, produces

$$H|\psi(0^-)\rangle = E_G |\psi(0^-)\rangle - \kappa |\psi_N^I\rangle \otimes |1\rangle \quad (\text{B1})$$

$$H^2|\psi(0^-)\rangle = (E_G^2 + \kappa^2) |\psi(0^-)\rangle - \kappa(E_G + E_N) |\psi_N^I\rangle \otimes |1\rangle \quad (\text{B2})$$

where $E_G = -Lh - \frac{\delta}{2}$, $E_N = -(L-2)h + \frac{\delta}{2}$ and $|\psi_N^I\rangle = |100\dots 0\rangle$. Replacing $|\psi_N^I\rangle \otimes |1\rangle$ in terms of $|\psi(0^-)\rangle$ using Eq. B1 we get,

$$[H^2 - (E_G + E_N)H - (\kappa^2 - E_G E_N)]|\psi(0^-)\rangle = 0 \quad (\text{B3})$$

From above we can obtain the following difference equation

$$F_{n+2} - (E_G + E_N)F_{n+1} - (\kappa^2 - E_G E_N)F_n = 0, \quad (\text{B4})$$

where $F_n = H^n |\psi(0^-)\rangle$ with initial conditions $F_0 = |\psi(0^-)\rangle$, $F_1 = E_G |\psi(0^-)\rangle - \kappa |\psi_N^I\rangle \otimes |1\rangle$. We can solve this difference equation using the characteristic root method. Let's assume a solution of this equation is of the form $F_n = \chi^n$, then the characteristic equation for the above difference equation is given by

$$\chi^2 - (E_G + E_N)\chi - (\kappa^2 - E_G E_N) = 0 \quad (\text{B5})$$

with two fundamental solutions,

$$\chi_{1,2} = \frac{(E_G + E_N) \pm \sqrt{(E_G + E_N)^2 + 4(\kappa^2 - E_G E_N)}}{2}. \quad (\text{B6})$$

The solution for this difference equation utilizing the initial conditions can be written as,

$$H^n |\psi(0^-)\rangle = \left[\frac{F_1 - \chi_2 F_0}{\omega} \right] \chi_1^n + \left[\frac{-F_1 + \chi_1 F_0}{\omega} \right] \chi_2^n \quad (\text{B7})$$

where

$$\omega = \sqrt{(E_G - E_N)^2 + 4\kappa^2} \quad (\text{B8})$$

The wavefunction $|\psi(t)\rangle = \exp(-iHt) |\psi(0^-)\rangle$ utilizing Eq. B7 to a global phase is,

$$\begin{aligned} |\psi(t)\rangle &= \sum_{n=0}^{\infty} \frac{(-it)^n}{n!} H^n |\psi_I\rangle \\ &= A(t) |\psi_G^I\rangle \otimes |0\rangle + B(t) |\psi_N^I\rangle \otimes |1\rangle, \\ A(t) &= \cos \frac{\omega t}{2} + i \frac{\delta + 2h}{\omega} \sin \frac{\omega t}{2}, B(t) = \frac{2i\kappa}{\omega} \sin \frac{\omega t}{2}. \end{aligned}$$

Appendix C: Evolution operator in the interaction picture: short time ($t \ll \kappa^{-1}$)

The Hamiltonian in Eq. 2 can be expressed as

$$H = H_0 + V_{Iq}, \text{ with } H_0 = H_I \otimes \mathbb{1}_q + \mathbb{1}_I \otimes H_q, \quad (\text{C1})$$

where H_0 is free part of the total Hamiltonian and V_{Iq} is the interaction Hamiltonian. The evolution operator in the interaction picture U_I can be written as

$$U_I(t, 0) = U_0^\dagger(t, 0) U_S(t, 0) \quad (\text{C2})$$

where we take the initial time as 0. $U_0(t, 0)$ is the evolution operator corresponding to the Hamiltonian H_0 and $U_S(t, 0)$ is the evolution operator in Schrödinger picture. Consequently,

$$U_I(t, 0) = e^{iH_0 t} e^{-iHt} \quad (\text{C3})$$

Using Baker–Campbell–Hausdorff expansion [76–78] and keeping terms only linear in time, we obtain

$$U_I(t, 0) \approx e^{i(H_0 - H)t} = e^{-iV_{Iq}t}. \quad (\text{C4})$$

This is consistent with the high-frequency approximation of evolution operator and time scale is identified in the inverse of the strength of V_{Iq} .

Appendix D: Derivation of initial growth of linear entropy for two qubits

For a very short time, the time evolution operator U can be approximated to

$$U \approx \mathbb{1} - iV_{Iq}t. \quad (\text{D1})$$

Applying this on $|\psi(0^-)\rangle = |\psi_G^I\rangle \otimes |00\rangle$ yields,

$$|\psi(t)\rangle \approx |\psi(0^-)\rangle + i\kappa t [|\phi_1^I\rangle \otimes |10\rangle + |\phi_2^I\rangle \otimes |01\rangle]. \quad (\text{D2})$$

The states $|\phi_1^I\rangle$ and $|\phi_2^I\rangle$ are obtained from the ground state of the Ising by flipping the Ising spins connected with the qubits. We rewrite the Eq. D2 as,

$$|\psi(t)\rangle \approx |\psi(0^-)\rangle + \sqrt{2}\kappa t |\psi_N^I\rangle, \quad (\text{D3})$$

with,

$$|\psi_N^I\rangle = \frac{1}{\sqrt{2}} [|\phi_1^I\rangle \otimes |10\rangle + |\phi_2^I\rangle \otimes |01\rangle]. \quad (\text{D4})$$

Since the Ising Hamiltonian commutes with parity, therefore, the states obtained by flipping single spin will be orthogonal to the ground state ($|\psi_N^I\rangle \perp |\psi_G^I\rangle$). The form of the time evolved state for one ancillary qubit for a short time is,

$$|\psi(t)\rangle = |\psi_I(t)\rangle + i\kappa t |\psi_N(t)\rangle. \quad (\text{D5})$$

From eq. D3 and eq. D5, we see that for two qubits if we redefine the quench parameter κ as $\sqrt{2}\kappa$, we will get the same form for the time-evolved state as for one qubit. One can easily show that such scaling of the interaction parameter still works if the initial state is maximally coherent. This is consistent with the scaling conjecture put forward in [48]. Therefore, we approximate the short time behaviour of linear entropy for n number of qubits by the same form as obtained for one qubit system by rescaling $\kappa \rightarrow \sqrt{n}\kappa$,

$$S_L = \frac{1}{4} [1 - \cos(4\sqrt{n}\kappa t)]. \quad (\text{D6})$$

Appendix E: Derivation of a complete transition to Lubkin value

The time-evolved state at the initial time can be Schmidt decomposed by using the unperturbed eigenstates as Schmidt eigenvectors. With increasing time, another unperturbed eigenstate energetically close to the earlier eigenstates will contribute, resulting in three prominent Schmidt eigenvalues. The process is continuously repeated which results in a fragmentation of Schmidt eigenvalues into smaller pieces. The purity of

the state is $\mu_2 = \text{tr} \rho_q^2$ where ρ_q is the reduced density matrix of qubits. Following the iteration scheme, the difference in purity between two consecutive iterations can be expressed as

$$\mu_2' - \mu_2 = -2\kappa^2 t^2 \mu_2 + 2\kappa^2 t^2$$

$$\frac{d\mu_2}{dt} = -4\kappa^2 t \mu_2 + 4\kappa^2 t$$

the continuum version using $\frac{t^2}{2} = \int t dt$

$$\frac{d(1 - \mu_2)}{dt} = -4\kappa^2 t (1 - \mu_2)$$

$$\frac{dS_L}{dt} = -4\kappa^2 t S_L.$$

We know that at $t \rightarrow \infty$, $S_L(t) \rightarrow S_L^\infty$, and as there is a steady state, time-derivative should vanish. S_L^∞ is the Lubkin value [47]. Therefore,

$$\frac{dS_L}{dt} = -4\kappa^2 t (S_L - S_L^\infty).$$

Also, note that $t \rightarrow 0$, slope should be $4\kappa^2 t$, and $S_L(t \rightarrow 0) \rightarrow 0$, therefore, we must divide by S_L^∞ . This motivates us to write the ‘‘correct’’ equation as,

$$\frac{dS_L}{dt} = -\frac{4\kappa^2 t}{S_L^\infty} (S_L - S_L^\infty) \quad (\text{E1})$$

which with initial condition $S_L(0) = 0$, yields the solution,

$$S_L(t) = \left[1 - \exp\left(-\frac{2\kappa^2 t^2}{S_L^\infty}\right) \right] S_L^\infty \quad (\text{E2})$$